

# Hydrogen-atom-assisted thione–thiol tautomerization of thiourea derivatives in *para*-H<sub>2</sub> matrix

Cite as: J. Chem. Phys. 162, 174306 (2025); doi: 10.1063/5.0265542

Submitted: 14 February 2025 • Accepted: 9 April 2025 •

Published Online: 2 May 2025



View Online



Export Citation



CrossMark

Sándor Góbi,<sup>1,2,a)</sup> Barbara Keresztes,<sup>1,3</sup> Anita Schneiker,<sup>1,3</sup> and György Tarczay<sup>1,2,4</sup>

## AFFILIATIONS

<sup>1</sup>Laboratory of Molecular Spectroscopy, Institute of Chemistry, ELTE Eötvös Loránd University, P.O. Box 32, H-1518 Budapest, Hungary

<sup>2</sup>MTA-ELTE Lendület Laboratory Astrochemistry Research Group, Institute of Chemistry, ELTE Eötvös Loránd University, P.O. Box 32, H-1518 Budapest, Hungary

<sup>3</sup>Hevesy György PhD School of Chemistry, Institute of Chemistry, ELTE Eötvös Loránd University, P.O. Box 32, H-1518 Budapest, Hungary

<sup>4</sup>Centre for Astrophysics and Space Science, ELTE Eötvös Loránd University, P.O. Box 32, H-1518 Budapest, Hungary

<sup>a)</sup>Author to whom correspondence should be addressed: [sandor.gobi@ttk.elte.hu](mailto:sandor.gobi@ttk.elte.hu)

## ABSTRACT

Thiourea (TU) and its *N*-methylated derivative, *N*-methyl thiourea (NMTU), were exposed to H atoms generated in cryogenic *para*-H<sub>2</sub> matrices. The reactions were followed online by FT-IR spectroscopy. The freshly deposited matrices exclusively contained the more stable thione tautomeric forms. However, upon exposure to H atoms, the peaks belonging to the precursor molecules clearly decreased along with the simultaneous appearance of new signals. These new bands could be attributed to the corresponding higher-energy thiol forms (in the case of TU) and, tentatively, to an intermediate radical (in both the TU and NMTU experiments). The radicals are suggested to be the H-atom-addition products of the TU and NMTU thione precursors, with the addition occurring on the S atom. These intermediates may then react with another free H atom, leading to the formation of the more energetic thiol tautomers, following an H-atom-abstraction process. As such, these radicals act as the centerpiece of the reaction scheme, enabling the thione–thiol tautomerization. This H-atom-assisted process is similar to that observed for the related molecule, thioacetamide. The interpretation of the experimental results was supplemented by quantum-chemical computations, which predicted all the above-mentioned reactions to be barrierless. The presence of H atoms opens a barrierless pathway; thus, the process does not necessarily require activation through irradiation (e.g., broadband UV). These findings point to the ubiquitous nature of the facile hydrogenation/dehydrogenation of the S atom, implying that thione–thiol tautomerization may occur easily.

© 2025 Author(s). All article content, except where otherwise noted, is licensed under a Creative Commons Attribution (CC BY) license (<https://creativecommons.org/licenses/by/4.0/>). <https://doi.org/10.1063/5.0265542>

## I. INTRODUCTION

The tautomerization processes of sulfurous compounds have been the focus of researchers' interest for a long time (e.g., Refs. 1–4). The matrix-isolation (MI) technique offers a convenient method to study chemical reactions that otherwise could not be followed. It has a vast literature in many different scientific fields, including the *in situ* isolation of radicals, conformational analysis and shifting of the conformational equilibrium, and observation of (photo)decomposition or tunneling reactions.<sup>5</sup> The sample

molecules are dispersed in a host material in a low concentration (generally 1:1000, but it depends on the matrix host); the high dilution and the inert environment result in negligible intermolecular interactions and smaller bandwidths (better spectral resolution). Traditionally, noble or other inert gases are used as matrix hosts (Ne, Ar, Kr, Xe, N<sub>2</sub>), but more reactive (e.g., CO) and more exotic (e.g., *para*-H<sub>2</sub>) matrices are also used. The MI technique is mostly coupled with an optical spectroscopic method (such as FT-IR spectroscopy) to exploit the better spectral resolution. The “quantum-solid” *para*-H<sub>2</sub> environment provides unique features, which make it superior

to other matrix hosts in some applications.<sup>6</sup> The interactions are even weaker, resulting in even narrower spectral bands. Furthermore, the matrix is considered to be soft compared to a noble gas host, allowing for the rapid diffusion of the *in situ* formed products, such as radicals. This so-called diminished cage effect reduces the likelihood of radical recombination, thus allowing for the observation of such molecules, which do not form in traditional matrices. The most interesting property of the *para*-H<sub>2</sub> matrix is that H atoms can be efficiently generated, which can effectively diffuse in this environment through the repetition of the  $H + H_2 \rightarrow H_2 + H$  tunneling reaction in solid *para*-H<sub>2</sub>.<sup>7</sup> Studies done in a *para*-H<sub>2</sub> matrix, involving the reactions with H atoms, have become routinely carried out by the groups of Anderson and Lee as well as in our laboratory, as evidenced by numerous studies in the past several years (e.g., Refs. 8–11).

Focusing on thioureas, it has long been known that thiourea (TU), exclusively existing in its more stable thione tautomeric form when deposited in an inert matrix, undergoes a thione to thiol tautomerization when exposed to radiation [e.g., broadband UV; Figs. 1(a) and 1(b)].<sup>12,13</sup> The photogenerated thiols had been observed to spontaneously convert back, due to H atom tunneling, to the lower-energy thione forms. The results were later confirmed by theoretical computations.<sup>14</sup> Recently, the N-methylated derivative, N-methyl thiourea [NMTU; Figs. 1(c)–1(h)], has also been investigated in the same manner, yielding similar results.<sup>15</sup> The tautomerization of the related thioamide (thioacetamide, TA) was also shown in cryogenic media upon UV irradiation.<sup>16</sup> More importantly, a later study pointed to the possibility of the occurrence of the thione–thiol tautomerization, without having to irradiate the matrix-isolated sample containing TA, by simply exposing it to H

atoms generated *in situ* in a *para*-H<sub>2</sub> matrix.<sup>17</sup> This experiment was also repeated in the low-temperature bulk (ice) phase by bombarding the TA sample with H atoms generated by an H atom beam source (HABS).<sup>18</sup> Our aim is to further examine the effect of H atoms on TU and NMTU samples, exploiting the unique feature of the *para*-H<sub>2</sub> matrix, in order to understand their tautomerization processes. The present study also reveals that the H-atom-assisted tautomerization appears to be ubiquitous for sulfurous compounds and not a unique feature of TA.

## II. MATERIALS AND METHODS

The MI experiments were conducted using the VIZSLA setup, comprising an ultrahigh-vacuum (UHV) compatible stainless steel simulation chamber with a base pressure of  $\approx 10^{-9}$  mbar when cooled.<sup>19</sup> *Para*-H<sub>2</sub> served as a matrix host, which was produced by converting *normal*-H<sub>2</sub> (Messer, 99.999%) on porous Fe(III) oxide [Sigma-Aldrich (St. Louis, MI, USA), hydrated, catalyst grade, 30–50 mesh] catalyst. The catalyst was filled into a stainless steel capillary wrapped around the “10 K” cryostat (CH202, Sumitomo Heavy Industries Inc.) of the setup, kept at 13.9 K. The *para*-H<sub>2</sub> was collected in a 0.5 L glass flask on a gas mixing line directly connected to the simulation chamber through a high-purity copper tube 6 mm in diameter.

The matrix was deposited by co-freezing TU (Sigma-Aldrich,  $\geq 99.0\%$ ) or NMTU (Sigma-Aldrich, 97%) and *para*-H<sub>2</sub> on a gold-plated silver wafer with an approximate surface area of 1 cm<sup>2</sup>, used as the substrate and attached to the cold finger of the “3 K” cryostat of the setup (RDK-415D, Sumitomo Heavy Industries Inc.). The

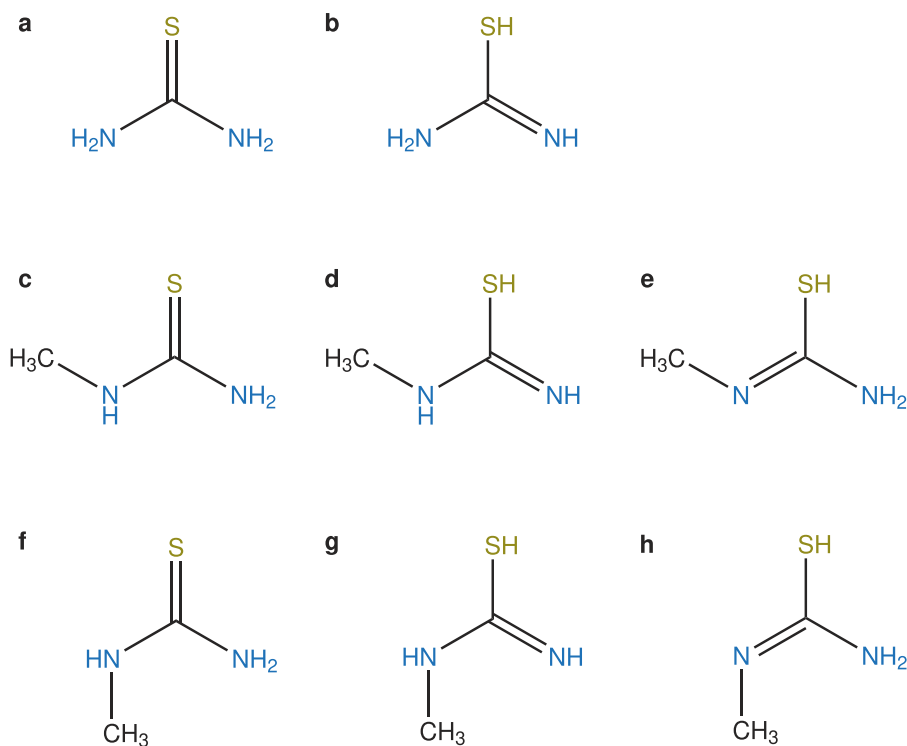


**FIG. 1.** Schematic representation of the tautomeric forms of the studied molecules: (a) TU amino-thione, (b) TU imino-thiol, (c) *syn*-NMTU amino-thione, (d) *syn*-NMTU imino-thiol, (e) *cis*-NMTU methylimino-thiol, (f) *anti*-NMTU amino-thione, (g) *anti*-NMTU imino-thiol, and (h) *trans*-NMTU methylimino-thiol.

precursors had been put into the heatable sample container of the setup before evacuating the chamber, and they were heated up to 353 and 345 K, maintained by a Lake Shore 336 temperature controller during deposition. The distance between the substrate and the tip of the sample container was  $\approx 3$  cm. The *para*-H<sub>2</sub> was let into the main chamber via a stainless steel capillary array through a leak valve; the distance between the substrate and the end of the capillaries was roughly 3 cm as well. The inlet rate was kept at  $\approx 0.8$  mbar L min<sup>-1</sup>. The matrix has to be doped with molecular Cl<sub>2</sub> for H atom generation, which was introduced using another leak valve and capillary array; the Cl<sub>2</sub> to *para*-H<sub>2</sub> ratio in the gas phase was roughly 1:400.

The H atoms were produced by applying the two-step process originally developed by Raston *et al.*<sup>8,9,20–22</sup> First, the deposited matrix was exposed to a 365 nm LED irradiation (M365L3 LED source, ThorLabs, *fwhm*  $\approx 9$  nm, supplied with an SM1U collimation adapter and a LEDD1B driver) for 30 + 15 minutes using a current of  $I = 0.25$  A to generate Cl atoms through Cl<sub>2</sub> dissociation. The exposure time was 30 + 30 minutes using a current of  $I = 0.25$  A in the case of NMTU. Owing to the diminished cage effect that can be experienced in *para*-H<sub>2</sub>, the Cl atoms may rapidly diffuse in the matrix, reducing the probability of recombination. This was followed by the 2217 nm (4510 cm<sup>-1</sup>) near-IR (NIR) laser excitation of the Q<sub>1</sub>(1) + S<sub>0</sub>(0) and Q<sub>1</sub>(0) + S<sub>0</sub>(0) combination bands of the *para*-H<sub>2</sub> molecules, enabling the Cl + *para*-H<sub>2</sub> reaction producing H and HCl. The 2217 nm irradiation was done with the help of an optical parametric oscillator (OPO, GWU/Spectra-Physics VersaScan MB 240, *fwhm*  $\approx 5$  cm<sup>-1</sup>) equipped with a frequency-doubling unit (Spectra-Physics uvScan) pumped by a pulsed Nd:YAG laser (Spectra-Physics Quanta Ray Lab 150,  $P \approx 1.9$ –2.0 W,  $\lambda = 355$  nm,  $f = 10$  Hz, pulse duration = 2–3 ns). The 2217 nm irradiation lasted 91 (TU) and 113 minutes (NMTU), respectively; the output power measured at the aperture of the OPO was  $P = 0.85$ –0.91 mJ (TU)

and 1.03–1.26 mJ (NMTU) per pulse. Then, the samples were kept in the dark overnight, and the H atom generation was repeated the next day. In the case of TU, the 365 nm LED irradiation took 30 + 30 min, applying a current of 0.33 A, followed by a 62-minute-long 2217 nm irradiation ( $P = 0.59$ –1.01 mJ per pulse). The matrix did not survive the 365 nm irradiation part of the second H atom generation in the NMTU experiment. The TU sample was also exposed to 240 nm laser irradiation (exposure time 30 min),  $P = 0.39$ –0.58 mJ per pulse.

Reflection-absorption mid-IR (MIR) spectra were collected by means of a Bruker Invenio FT-IR spectrometer equipped with a liquid N<sub>2</sub>-cooled mid-band Mercury Cadmium Telluride (MCT) detector. The data were saved in the spectral region of 4000–600 cm<sup>-1</sup> at a resolution of 0.5 cm<sup>-1</sup>, averaging 32 scans each minute during deposition and during the 2217 nm as well as the 240 nm laser irradiations. A low-pass filter with a cutoff wavenumber of 3860 cm<sup>-1</sup> was inserted after deposition to hinder the interference between the 2217 nm laser photons with the MCT detector. After the NIR irradiation, the changes in the sample when it was kept in the dark were monitored by taking 128 scans every 30 min. Long, 128-scan spectra were also collected right after deposition, the 365 nm LED and the 240 nm laser UV irradiations, as well as after waiting 2 h after finishing all the irradiation studies in the case of the TU sample. MIR background spectra, averaging 256 scans, with and without the cutoff filter, were taken right before the sample deposition at the same temperature and resolution as during the experiment. A 32-scan NIR spectrum was collected after preparing the matrix to calculate the *ortho*-H<sub>2</sub> mixing ratio (i.e., the purity) as well as the optical path length of the *para*-H<sub>2</sub> matrix. The optical path length is important for determining the mixing ratios of the matrix-isolated species. NIR spectra averaging 32 scans were also saved during and after the 365 nm irradiation, as well as after the 2217 nm irradiation, to follow the formation or destruction

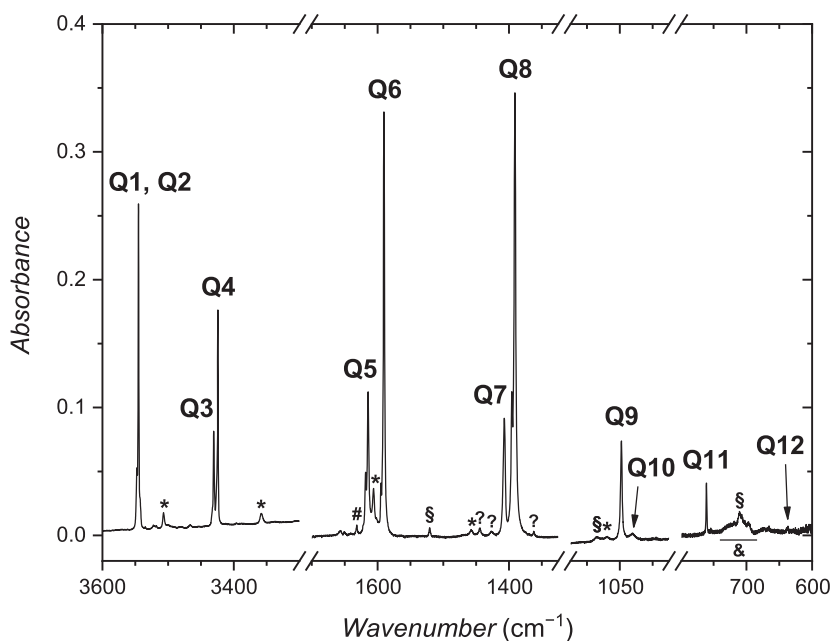


**FIG. 2.** MIR spectrum of TU deposited in *para*-H<sub>2</sub>, whose vibrational modes are marked with Q<sub>n</sub> (where  $n = 1$ –14; the notation is taken from Ref. 12). The symbols mark the following absorption bands: \*: Cl<sub>2</sub> complexes with TU; #: *para*-H<sub>2</sub>O;<sup>6</sup> §: band assigned to TU by Ref. 12, but no specific vibrational mode was given; ?: band also seen in the spectra of Ref. 12 but not listed in the assignment table; and &: broad S<sub>0</sub>(0) + S<sub>0</sub>(0) band of *para*-H<sub>2</sub>.<sup>27</sup>

of Cl atoms. The NIR background of 128 scans was also obtained before the experiment.

Quantum-chemical DFT computations were also carried out with the Gaussian 16 software (Rev. A03).<sup>23</sup> The geometry optimization of the precursor, as well as possible products and transition states (TSs), took place at the B3LYP/cc-pV(T+d)Z level of theory. The same level of theory was used to obtain the harmonic and anharmonic vibrational frequencies and intensities, utilizing the vibrational perturbation theory (VPT2) for the anharmonic computations.<sup>24,25</sup>

### III. EXPERIMENTAL RESULTS

#### A. H-atom reaction studies

The spectra of TU dispersed in a cryogenic *para*-H<sub>2</sub> matrix agree well with those obtained previously (Fig. 2).<sup>26</sup> The only difference is the appearance of a few extra peaks due to the presence of Cl<sub>2</sub> in the matrix (used for H atom generation). It is important to note that these signals are absent in the “blank” experiment when the matrix does not contain any Cl<sub>2</sub> molecules. The most straightforward explanation for these peaks is the formation of weakly bound Cl<sub>2</sub> complexes with the precursor molecule, perturbing its vibrational band positions. Such bands can be found at 3507.0 (corresponding to the Q1 and Q2 bands of the TU thione precursor; notation taken from Ref. 12), 3358.4 (Q3 and Q4), 1618.2 (Q5), 1606.1 (Q6), 1457.6 (Q7), 1395.7 (as shoulder, Q8), and 1069.5 cm<sup>-1</sup> (Q9). An alternative assignment would be the direct reaction of Cl<sub>2</sub> with the precursor molecule, leading to the formation of chlorinated products. These bands almost completely disappear by the end of the 365 nm irradiation, showing the photolability of the molecule accounting for them.

During and after H atom generation, a whole set of new peaks emerges (Fig. 3). The position of these signals is in great agreement with those of the thiol tautomeric forms of TU and, thus, can be safely assigned to them. The assignment can be done by comparing the results with previous experimental data obtained in *para*-H<sub>2</sub> when TU was irradiated by selective laser UV photons.<sup>26</sup> As such, the bands with the maxima at 3527.4, 1644.0, 1321.2, and 1071.8 cm<sup>-1</sup> are ascribable to the *s(yn),t(rans)*-thiol, whereas the peaks at 3530.5, 1653.5, 1298.1, 1121.3, and 1080.2 cm<sup>-1</sup> are caused by the absorption of the *s,c(is)*-thiol tautomer of TU (Fig. 4). Note that there are four different rotamers; the other two are denoted as *a(anti),c*- and *a,t*-thiol, based on the relative orientation of the H atoms of the -SH (*s*- or *a*- along the H-S-C=N dihedral angle) as well as the =NH (*c* or *t* position of the S-C=N-H dihedral angle) moieties. However, similarly to the work of Rostkowska *et al.*,<sup>12</sup> only the *s,c*- and *s,t*-thiol rotamers are considered by this study, as the computed vibrational frequencies of the *a,c*-thiol are indistinguishably close to those of the *s,c*-thiol, and the same applies to the *a,t* and *s,t* isomers. One more peak that apparently increases during the whole H-atom reaction can be found at 968.3 cm<sup>-1</sup> and is due to the forming NH<sub>3</sub> molecule.<sup>28</sup> Even more interestingly, a triplet band with maximum positions of 2323.7, 2321.7, and 2319.0 cm<sup>-1</sup> shows up during the first H atom generation (2217 nm irradiation, Fig. S1 in the [supplementary material](#)). This feature stays stable in the dark and becomes completely bleached during the second 365 nm irradiation; however, it is regenerated during the repeated 2217 nm irradiation. Even though this behavior is difficult to properly monitor owing to the interference with the atmospheric CO<sub>2</sub>, it still shows a resemblance to that of the 2378 cm<sup>-1</sup> signal in a similar experiment carried out with TA.<sup>17</sup> In that work, the molecule accounting for the 2378 cm<sup>-1</sup> band was tentatively identified as an important intermediate produced following the H-atom addition on the S atom of TA.

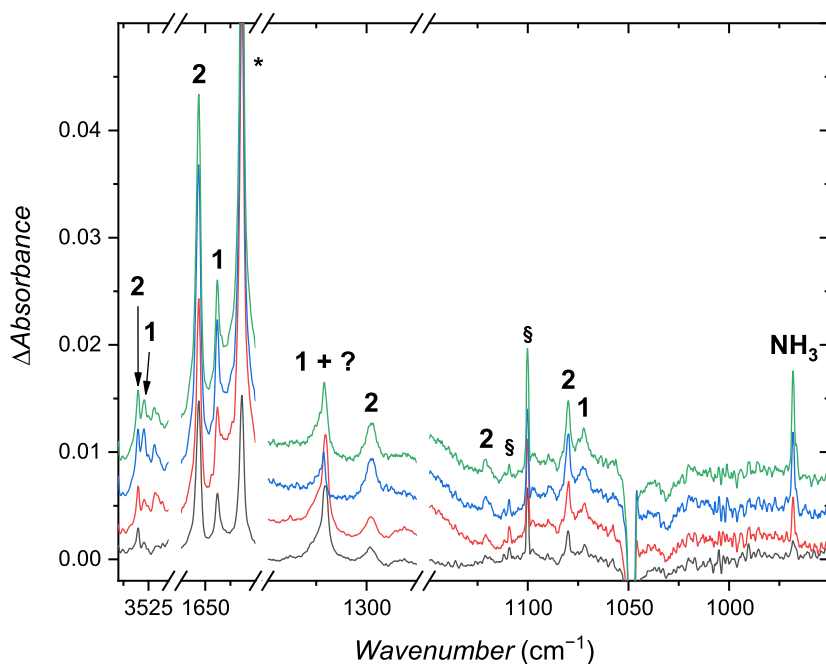


**FIG. 3.** Sections of the MIR difference spectra of TU in *para*-H<sub>2</sub> matrix after the first H atom generation (dark gray trace), the next day after keeping the sample in the dark (red trace), after the second 365 nm irradiation (blue trace), and after the second 2217 nm irradiation (green trace). The spectrum taken right after deposition serves as the reference for the difference spectra. The spectra are offset for clarity; labels “1” and “2” denote the *s,t*- and the *s,c*-thiol rotamers. The asterisk marks the forming *para*-H<sub>2</sub>O band, whereas the “§” symbols label the HO· radical; both species are standard by-products upon H atom generation. The question mark signals an uncertain assignment. The position of the NH<sub>3</sub> absorption band is also shown.

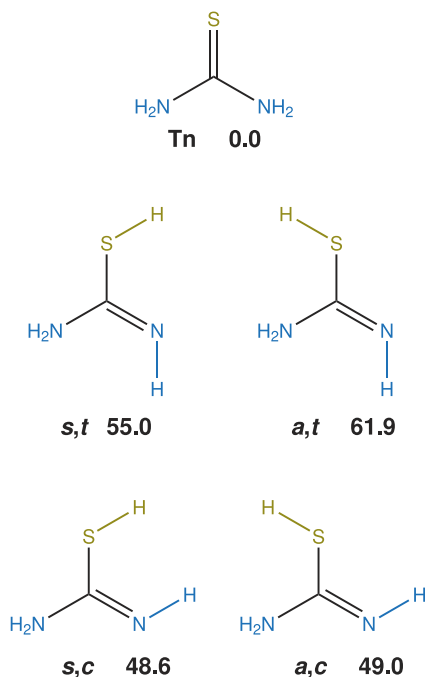


**FIG. 4.** Schematic representation of the different thiol rotamers of TU. For the sake of comparison, the thione tautomeric form (Tn) is also shown. The energies relative to that of Tn as obtained at the B3LYP/cc-pV(T+d)Z level of theory are also provided (in  $\text{kJ mol}^{-1}$ ), which are zero-point vibrational energy (ZPVE) corrected.

The subsequent 240 nm secondary photolysis, which was meant to support the identification process, induces further changes in the spectrum. All TU bands (including both the thione and thiol forms) start decreasing, pointing to their decomposition, whereas that of the  $\text{NH}_3$  increases, and numerous new bands appear according to the TU decomposition products. These are hydrogen isocyanide (HNC), isothiocyanic acid (HNCS), cyanamide ( $\text{H}_2\text{N}-\text{CN}$ ), carbodiimide ( $\text{HN}=\text{C}=\text{NH}$ ), and hydrogen cyanide (HCN), whose formation is in accordance with a previous photolytic study.<sup>26</sup>

When taking the MIR spectrum of NMTU in a *para*- $\text{H}_2$  matrix, one can deduce the same as in the case of TU; the spectrum agrees well with the previously obtained one (Fig. S2 in the [supplementary material](#)).<sup>26</sup> The fact that both the *s*(yn) and *a*(nti) conformers are present in the matrix is in complete accordance with previous results.<sup>15,26</sup> Similarly to the TU experiment, the presence of  $\text{Cl}_2 \cdots \text{NMTU}$  complexes (or, alternatively, chlorinated products) can also be observed. However, unlike in the experiment done with TU, no formation of NMTU thiols can be detected upon the generation of H atoms in the matrix. It should be noted that the position of the thiol absorption bands is also well known based on a recent UV photolytic study carried out in a *para*- $\text{H}_2$  matrix.<sup>26</sup> The only new band that appears has a maximum of  $2329.9 \text{ cm}^{-1}$  (Fig. S3 in the [supplementary material](#)). This peak shares similar behavior to the signal centered at  $2378 \text{ cm}^{-1}$  in the case of TA or to the triplet band in the TU experiment. Thus, it is reasonable to assume that it is the same type of reaction product as that of TA or TU; namely, the radical that is produced when an H-atom addition reaction occurs on the S atom.

## B. Kinetics of TU tautomerization

The kinetic curves were initially obtained by plotting the integrated peak band areas ( $A(\tilde{\nu})$ , in  $\text{cm}^{-1}$ ) vs time. It is important to point out that the use of band areas has disadvantages, as they are not normalized by the different absorption coefficients of the different vibrational modes or the thickness of the matrix. One often applied solution for that is the use of the mixing ratio of the components with regard to the matrix host ( $X$ , in ppm), for which the following equation is used:<sup>6</sup>

$$X = 2.303 \int_{\text{band}} \frac{A(\tilde{\nu}) d\nu}{\epsilon l} \times V_{\text{mol}} \times 10^6.$$

The method was successfully adopted by our group and has been utilized in numerous works since then.<sup>29</sup> The optical path of the IR beam in the deposited *para*- $\text{H}_2$  matrix ( $l$ , in cm), which is a fundamental value to determine the mixing ratio of each species, is calculated to be  $0.0261 \pm 0.008 \text{ cm}$  using the updated coefficients provided by Fajardo.<sup>30</sup> To estimate the absorption coefficient ( $\epsilon$ , in  $\text{cm mol}^{-1}$ ), the computed IR intensities are used. It is important to note that, based on previous results, the use of harmonic computed IR intensities is preferred over the anharmonic ones. This is due to the unreliable manner of the latter, especially in the case of low-frequency vibrational modes of “floppy” functional groups (such as the torsional mode of the methyl, i.e., the  $-\text{CH}_3$ , group).<sup>26</sup>

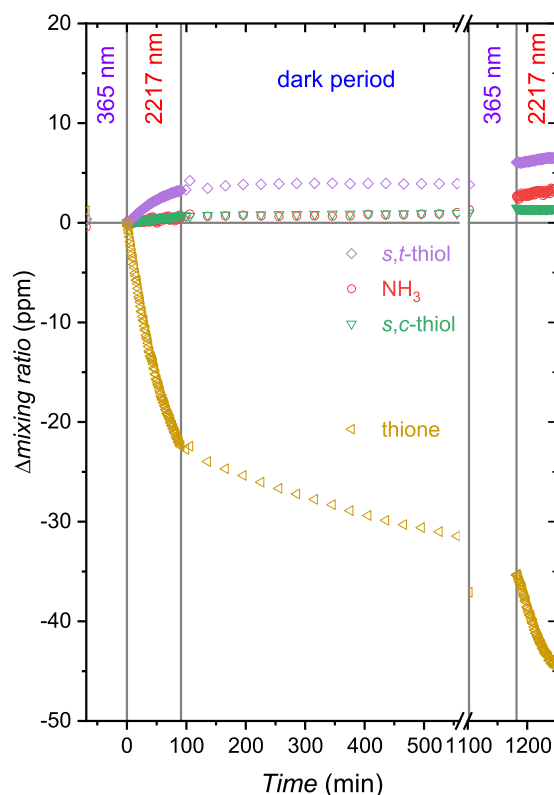


**FIG. 5.** Kinetic curves of TU thione and thiol tautomers as well as that of  $\text{NH}_3$  during H atom generation. The vertical lines mark the boundaries between the different stages of the experiment.

Finally,  $V_{\text{mol}}$  is the molar volume of solid *para*-H<sub>2</sub>, equaling 23.16 cm<sup>3</sup> mol<sup>-1</sup>, and the factor of 10<sup>6</sup> ensures the mixing ratio is obtained in ppm units.

To estimate the mixing ratio of the TU thione precursor, two vibrational modes were considered: the NH<sub>2</sub> in-phase bending ( $\beta_{\text{ip}}[\text{NH}_2]$ , **Q6**), centered at 1590.3 cm<sup>-1</sup> with a computed harmonic IR intensity of 206 km mol<sup>-1</sup>, and the NH<sub>2</sub> out-of-phase bending ( $\beta_{\text{op}}[\text{NH}_2]$  or **Q5**, 1614.5 cm<sup>-1</sup>, 69 km mol<sup>-1</sup>). Due to the low concentration of the products resulting in weak absorptions, only one vibrational mode could be considered for the thiols and NH<sub>3</sub>. These were the C=N stretching ( $\nu[\text{C}=\text{N}]$ ) in the case of thiols: 1644.0 cm<sup>-1</sup> (271 km mol<sup>-1</sup>) and 1653.5 cm<sup>-1</sup> (253 km mol<sup>-1</sup>) for the *s,t* and *s,c* conformers. The decomposition product NH<sub>3</sub> has one strong band at 968.3 cm<sup>-1</sup> (147 km mol<sup>-1</sup>), which can be assigned to its wagging mode ( $\omega[\text{NH}_3]$ ). The kinetic profile of the triplet band at 2323.7, 2321.7, and 2319.0 cm<sup>-1</sup> could not be determined due to the strong interference with the absorption of the atmospheric CO<sub>2</sub> residue that can be found in the IR beam path.

As far as the kinetic behavior of the TU thione tautomeric form is concerned, it can be seen from Fig. 5 that its mixing ratio monotonously decreases during all stages of the H-atom reaction. This conversion is more pronounced when the sample is exposed to 2217 nm laser photons. The loss rate is lower when the sample is kept in the dark, although still non-negligible. In contrast, the

precursor is apparently not affected by the 365 nm irradiation. In summary, some ≈20 ppm of TU thione is transformed in the first 2217 nm irradiation, followed by the conversion of 15 ppm more in the dark, and eventually, another 10 ppm is converted when the sample is exposed to the NIR photons for the second time. In contrast, the mixing ratio of the products increases monotonously, although at different rates. For instance, the concentration of *s,c*-thiol is low throughout the experiment: it is calculated to be a mere 0.7 ppm after the first 2217 nm irradiation and is not much higher by the end of the dark period (1.0 ppm). Then, it slightly increases during the second 365 nm LED irradiation to ≈1.5 ppm and eventually remains more or less stable during the second NIR laser irradiation. The mixing ratio of the other rotamer, the *s,t*-thiol, has a somewhat higher overall mixing ratio: 3.2 ppm at the end of the first H atom generation cycle and 3.8 ppm after waiting 1012 min in the dark. This value almost doubles to 6.1 ppm after the second 365 nm LED irradiation and increases further to 6.5 ppm during the second 2217 nm laser irradiation. Even though the *s,t*-thiol rotamer is known for its back-conversion to the TU thione tautomeric form via an intramolecular H atom tunneling, its half-life was found to be 52 h in Ar, 76 h in Ne, and 94 h in *normal*-H<sub>2</sub>,<sup>12,13</sup> which can be offset by the reactions of the TU thione with the remaining H atoms left in the dark. To summarize, the kinetic behavior of TU thiols shows a great resemblance to that of the TA thiols upon H atom generation.<sup>17</sup> Finally,

**TABLE I.** ZPVE-corrected relative energies ( $\Delta E_{\text{ZPVE}}$ ) and barrier heights [ $\Delta E(\text{TS})_{\text{ZPVE}}$ ; both in kJ mol<sup>-1</sup>] of all possible reaction steps of the TU thione and thiol tautomers as well as those of the H<sub>2</sub>N- $\dot{\text{C}}(-\text{SH})\text{NH}_2$  intermediate.

Process	Expected product	$\Delta E_{\text{ZPVE}}$	TS found?	$\Delta E(\text{TS})_{\text{ZPVE}}$
Compound: Thione				
H addition on S	H <sub>2</sub> N- $\dot{\text{C}}(-\text{SH})-\text{NH}_2$	-73.0	...	...
H addition on C	H <sub>2</sub> N-CH(- $\dot{\text{S}}$ )-NH <sub>2</sub>	-61.3	✓	26.2
S <sub>H</sub> 2 on NH <sub>2</sub>	H <sub>2</sub> N- $\dot{\text{C}}(=\text{S}) + \text{NH}_3$	6.3	✓	43.4
H abstraction from NH <sub>2</sub> #1	<i>cis</i> -H <sub>2</sub> N-C(=S)- $\dot{\text{N}}\text{H} + \text{H}_2$	-51.6	✓	13.4
H abstraction from NH <sub>2</sub> #2	<i>trans</i> -H <sub>2</sub> N-C(=S)- $\dot{\text{N}}\text{H} + \text{H}_2$	-28.6	✓	28.6
Compound: H <sub>2</sub> N- $\dot{\text{C}}(-\text{SH})\text{NH}_2$				
H addition on C	H <sub>2</sub> N-CH(-SH)-NH <sub>2</sub>	-326.1	...	...
H abstraction from SH	thione + H <sub>2</sub>	-361.3	...	...
H abstraction from NH <sub>2</sub>	<i>a,t</i> -thiol + H <sub>2</sub>	-299.4	...	...
Compound: <i>a,t</i> -thiol				
S <sub>H</sub> 2 substitution on SH	H <sub>2</sub> N- $\dot{\text{C}}=\text{NH} + \text{H}_2\text{S}$	-93.4	✓	6.5
H addition on C	H <sub>2</sub> N-CH(-SH)- $\dot{\text{N}}\text{H}_2$	-74.3	✓	40.8
S <sub>H</sub> 2 substitution on NH <sub>2</sub>	HN= $\dot{\text{C}}$ -SH + NH <sub>3</sub>	-86.1	✓	51.9
H addition on NH	H <sub>2</sub> N- $\dot{\text{C}}(-\text{SH})-\text{NH}_2$	-134.9	✓	2.9
H abstraction from SH	H <sub>2</sub> N-C(- $\dot{\text{S}}$ )=NH + H <sub>2</sub>	-90.5	...	...
H abstraction from NH <sub>2</sub> #1	<i>a,a</i> -HN- $\dot{\text{C}}(-\text{SH})=\text{NH} + \text{H}_2$	-34.9	✓	26.6
H abstraction from NH <sub>2</sub> #2	<i>s,a</i> -HN- $\dot{\text{C}}(-\text{SH})=\text{NH} + \text{H}_2$	-40.0	✓	33.3
H abstraction from NH	H <sub>2</sub> N-C(-SH)= $\dot{\text{N}} + \text{H}_2$	-57.2	✓	1.5

one should discuss the kinetic profile of  $\text{NH}_3$  as well: its mixing ratio is 0.6, 1.3, 2.6, and 3.5 ppm after the first 2217 nm irradiation, after waiting in the dark, after the second 365 nm irradiation, and at the end of the H atom generation.

#### IV. COMPUTATIONAL RESULTS

##### A. H-atom reactions of TU

When an H atom approaches a molecule, it can participate either in H-abstraction or H-addition reactions. In the case of the former, the incoming H atom may grab another one from the molecule and form an  $\text{H}_2$  molecule along with the remaining species with one less H atom. The possible sites for the H abstraction are the two amino ( $-\text{NH}_2$ ) groups, which are identical due to molecular symmetry. However, the H atoms on a particular  $-\text{NH}_2$  moiety are not identical, leading to two different barriers for the two H-abstraction reactions (13.4 and 28.6  $\text{kJ mol}^{-1}$ ). The barrier heights of the reaction steps of the most important species are listed in Table I, whereas all considered H-abstraction as well as H-addition reactions are discussed in the [supplementary material](#) and listed in Table S1 in the [supplementary material](#). The product of the H-atom-abstraction reaction involving the TU thione form is formally the aminothioxomethyl amidogen [ $\text{H}_2\text{N}-\text{C}(=\text{S})-\dot{\text{N}}\text{H}$ ] radical, although it may exist in another resonance structure, the aminoimino methylthio [ $\text{H}_2\text{N}-\text{C}(\dot{\text{S}})=\text{NH}$ ] radical. In contrast, the addition of the generated H atoms can occur on three possible targets on the TU thione form, namely, on the S as well as the C atoms and on one of the  $-\text{NH}_2$  moieties. In the last case, a bimolecular homolytic substitution ( $\text{S}_{\text{H}2}$ ) reaction takes place, resulting in the elimination of ammonia ( $\text{NH}_3$ ) and the aminothioxo methyl ( $\text{H}_2\text{N}-\dot{\text{C}}=\text{S}$ ) radical. This reaction channel and the one involving the H-atom addition on the C atom

have considerable barriers (43.4 and 26.2  $\text{kJ mol}^{-1}$ ). On the other hand, the addition of H atoms on the S atom is a barrierless process, yielding the diaminomercapto methyl [ $\text{H}_2\text{N}-\dot{\text{C}}(-\text{SH})-\text{NH}_2$ ] radical. Briefly, only the last reaction is expected to take place since all other ones have considerable barrier heights. These findings are in line with those of earlier studies focusing on the related molecule, TA.<sup>17,31</sup>

Considering the further reactions of the only species that forms after a barrierless process [ $\text{H}_2\text{N}-\dot{\text{C}}(-\text{SH})-\text{NH}_2$ ], it may also participate in H-addition or H-abstraction reactions. Among the possibilities, only the addition of the H atom on the C atom with the radical center is found to be barrierless in each case, yielding the fully hydrogenated diamino methanethiol [ $\text{H}_2\text{N}-\text{CH}(-\text{SH})-\text{NH}_2$ ] molecule. Speaking of the H-atom abstraction from the  $\text{H}_2\text{N}-\dot{\text{C}}(-\text{SH})-\text{NH}_2$  radical, the attacked H atoms can be either on the N atom of one of the  $-\text{NH}_2$  groups or the S atom of the  $-\text{SH}$  group, respectively. Both reactions are found to be barrierless by theory; the predicted products are the thiol and the thione tautomeric forms of TU, respectively.

The formation of thiols can be undoubtedly observed; therefore, it is imperative to assess their possible H-atom-reaction pathways. The addition on the S atom of the  $-\text{SH}$  group is found to have negligible barriers for three out of the four thiol conformers (ranging between 2.4 and 6.5  $\text{kJ mol}^{-1}$ ; the only exception is the *a,c*-thiol, for which a surprisingly high barrier of 39.1  $\text{kJ mol}^{-1}$  is predicted). This  $\text{S}_{\text{H}2}$  reaction leads to  $\text{H}_2\text{S}$  elimination. Similarly, the H-addition on the  $=\text{NH}$  group also has low barriers of 1.4–2.9  $\text{kJ mol}^{-1}$  (when found), which are lower than the uncertainty of the applied level of theory. This pathway allows the formation of the important  $\text{H}_2\text{N}-\dot{\text{C}}(-\text{SH})-\text{NH}_2$  intermediate. The addition on the C atom [producing the  $\text{H}_2\text{N}-\text{CH}(-\text{SH})-\dot{\text{N}}\text{H}$  radical] as well as

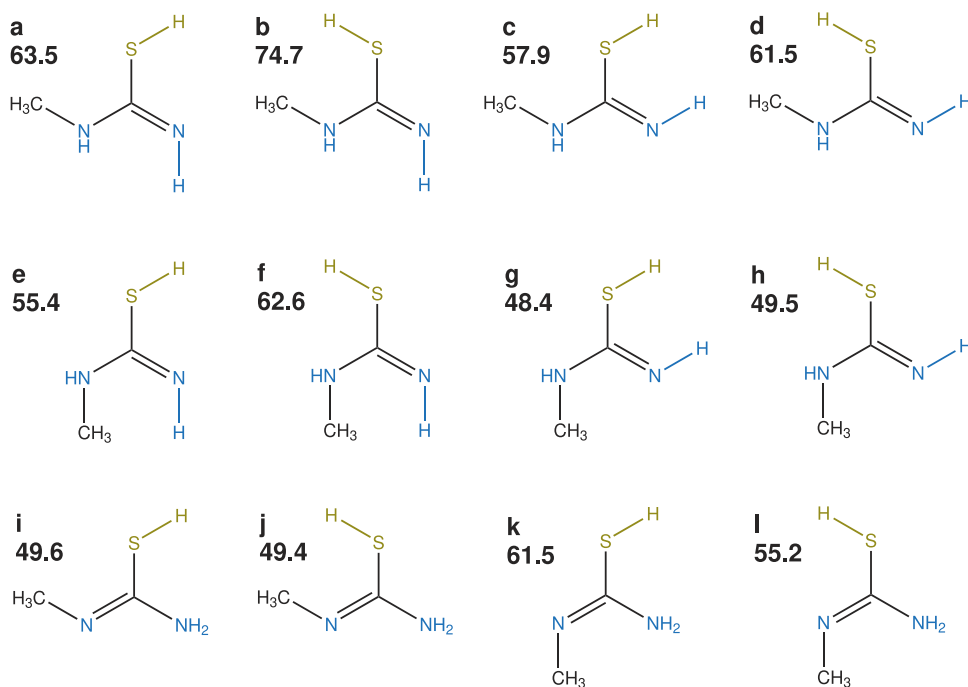


**FIG. 6.** Schematic representation of the different thiol rotamers of NMTU: (a) *s,s,t*-imino-thiol, (b) *s,a,t*-imino-thiol, (c) *s,s,c*-imino-thiol, (d) *s,a,c*-imino-thiol, (e) *a,s,t*-imino-thiol, (f) *a,a,t*-imino-thiol, (g) *a,s,c*-imino-thiol, (h) *a,a,c*-imino-thiol, (i) *a,c*-methylimino-thiol, (j) *s,c*-methylimino-thiol, (k) *a,t*-methylimino-thiol, and (l) *s,t*-methylimino-thiol. The ZPVE-corrected relative energies as obtained at the B3LYP/cc-pV(T+d)Z level of theory are also provided (in  $\text{kJ mol}^{-1}$ ); the reference is the *anti*-NMTU thione tautomer.

the addition on the N atom of the  $-\text{NH}_2$  moiety (involving the  $\text{NH}_3$  elimination following the  $\text{S}_{\text{H}2}$  mechanism) both have barriers higher than  $40 \text{ kJ mol}^{-1}$ . Out of the reactions involving H abstraction, only that occurring on the S atom of the  $-\text{SH}$  group is found barrierless by theory, formally resulting in the formation of the  $\text{H}_2\text{N}-\dot{\text{C}}(-\text{S})=\text{NH}$  radical (see the other resonance structure above). The abstraction of an H atom from the  $-\text{NH}_2$  group has barriers of  $25\text{--}40 \text{ kJ mol}^{-1}$ , depending on the thiol conformer. The same values for the reaction involving the  $=\text{NH}$  moiety are lower, around  $10 \text{ kJ mol}^{-1}$ . The only exception is the *s,t*-thiol, for which the same reaction has a negligible,  $1.2 \text{ kJ mol}^{-1}$  high barrier. The product of this reaction channel is the  $\text{H}_2\text{N}-\dot{\text{C}}(-\text{SH})=\dot{\text{N}}$  radical, which, on the other hand, can quickly react with an H atom, regenerating the thiol forms.

## B. H-atom reactions of NMTU

When discussing the processes taking place when the NMTU sample is exposed to H atoms, one should bear in mind that the number of conformers is much higher than in the case of TU. As such, the NMTU thione tautomeric form has two [*syn* and *anti*, Figs. 1(c) and 1(f)], whereas the thiol forms have 12 enantiomeric pairs (24 in all, Fig. 6) due to the fact that the  $-\text{SH}$  and  $=\text{NH}$  groups are out of the molecular plane. The first letter in the notation always describes the orientation of the  $-\text{CH}_3$  group, as discussed in Sec. I. In the case of the imino-thiol conformers [Figs. 6(a)–6(h)], the relative orientation of the H atoms of the  $-\text{SH}$  (*a* or *s* along the  $\text{H}-\text{S}-\text{C}=\text{N}$  dihedral angle) as well as the  $=\text{NH}$  (*c* or *t* along the  $\text{S}-\text{C}=\text{N}-\text{H}$  dihedral angle) groups are denoted by the second and the third letters in their notation. In the case of the methylimino-thiol tautomers [Figs. 6(i)–6(l)], only the former needs to be used, namely, the orientation of the H atom of the  $-\text{SH}$  (*a* or *s* along the  $\text{H}-\text{S}-\text{C}=\text{N}$  dihedral angle) group to properly describe the conformer structure (first letter of the notation, whereas the first letter denotes the relative orientation of the  $-\text{CH}_3$  group). Due to the high number of conformers, a comprehensive study was out of the scope of this work. Accordingly, only the most relevant reaction pathways are highlighted in order to test the feasibility of the thione–thiol tautomerization process (Table S2 in the supplementary material). The results point to the barrierless nature of the H addition on the S atom of the NMTU thione, yielding the intermediate radical  $[\text{H}_3\text{C}-\text{NH}-\dot{\text{C}}(-\text{SH})-\text{NH}_2]$ . In contrast, the H-atom abstraction has an average barrier of roughly  $20 \text{ kJ mol}^{-1}$  in every case, rendering the occurrence of these channels unlikely. The  $\text{H}_3\text{C}-\text{NH}-\dot{\text{C}}(-\text{SH})-\text{NH}_2$  radical may then lose an H atom through a barrierless H-atom abstraction, leading to the formation of the NMTU thiol conformers. It is important to point out that all of the H-abstraction processes are barrierless, independent of whether the H atom is located in the  $-\text{NH}-$  or  $-\text{NH}_2$  group.

## V. DISCUSSION

### A. Proposed tautomerization mechanisms

Figure 7 shows the most likely reaction mechanism that occurs upon exposing the TU sample to H atoms in a cryogenic *para*- $\text{H}_2$  matrix, deduced from both the experimental and theoretical results. According to the computational results disclosed in Sec. IV A, the TU thione tautomeric form may participate in a barrierless H-atom addition on the S atom. The resulting intermediate,  $\text{H}_2\text{N}-\dot{\text{C}}(-\text{SH})-\text{NH}_2$ , acts as the cornerstone of the thione–thiol

tautomerization mechanism and can be tentatively assigned by IR spectroscopy via its triplet band with maximum positions of  $2323.7$ ,  $2321.7$ , and  $2319.0 \text{ cm}^{-1}$ . This radical is proposed to transform barrierlessly into one of the thiol forms following an H-atom abstraction; their presence is undoubtedly confirmed experimentally. The theory also predicts the H-atom addition on the C atom of the  $\text{H}_2\text{N}-\dot{\text{C}}(-\text{SH})-\text{NH}_2$  radical to be barrierless, resulting in the formation of the fully hydrogenated  $\text{H}_2\text{N}-\text{CH}(-\text{SH})-\text{NH}_2$  molecule, although it cannot be observed in the IR spectrum. This could be due to the occurrence of the opposite reaction, namely, the dehydrogenation of this species upon H-atom abstraction, yielding the  $\text{H}_2\text{N}-\dot{\text{C}}(-\text{SH})-\text{NH}_2$  radical. Another reaction that probably takes place, although there is no evidence for it, is the regeneration of the  $\text{H}_2\text{N}-\dot{\text{C}}(-\text{SH})-\text{NH}_2$  intermediate following the hydrogenation of the thiol forms when an incoming H atom is barrierlessly added on their  $=\text{NH}$  groups. The presence of other species forming through barrierless processes, such as  $\text{H}_2\text{N}-\text{CH}(-\dot{\text{S}})-\text{NH}_2$  or  $\text{H}_2\text{N}-\text{C}(-\dot{\text{S}})=\text{NH}$ , is not expected owing to too low concentration—their formation from the initial thione tautomer requires too many hydrogenation/dehydrogenation steps.

The reactions of an incoming H atom with NMTU are expected to be analogous to what happens to TU. The H-atom addition on the S atom of the NMTU thione is expected to take place based on the computational results. The occurrence of this process is independent of whether the thione possesses the *anti* or *syn* structure. Then the forming intermediate, the tentatively detected (through its  $2329.9 \text{ cm}^{-1}$  band)  $\text{H}_3\text{C}-\text{N}(\text{H})-\dot{\text{C}}(-\text{SH})-\text{NH}_2$  radical, participates in a barrierless H-atom abstraction, producing the NMTU thiol tautomers. The fact that the NMTU thiols cannot be observed in the sample exposed to H atoms can be rationalized (among others) by their very low concentration, which may be caused by the high number of unique conformers (12 enantiomeric pairs, as stated above, in contrast to the two detected ones in the case of TU) rendering their signals below the detection limit.

The  $\text{CH}_3-\dot{\text{C}}(-\text{SH})-\text{NH}_2$  radical forming in the experiment starting from TA has a computed IR frequency and intensity of  $2311 \text{ cm}^{-1}$  and  $103 \text{ km mol}^{-1}$ .<sup>17</sup> The same values in the case of TU are  $2220 \text{ cm}^{-1}$  and  $168 \text{ km mol}^{-1}$  [ $\text{H}_2\text{N}-\dot{\text{C}}(-\text{SH})-\text{NH}_2$ ]; also compare it with the frequencies of the NMTU derivatives:  $2251 \text{ cm}^{-1}$  and  $161 \text{ km mol}^{-1}$  [*a*- $\text{H}_3\text{C}-\text{N}(\text{H})-\dot{\text{C}}(-\text{SH})-\text{NH}_2$ ] and  $2237 \text{ cm}^{-1}$  and  $144 \text{ km mol}^{-1}$  [*s*- $\text{H}_3\text{C}-\text{N}(\text{H})-\dot{\text{C}}(-\text{SH})-\text{NH}_2$ ]. In other words, they are shifted toward lower wavenumbers with regard to the similar experiment carried out by TA, which is also reflected in the experimental frequencies of these radicals:  $2378 \text{ cm}^{-1}$  (TA),  $2321.7 \text{ cm}^{-1}$  (TU; highest peak of the triplet), and  $2329.9 \text{ cm}^{-1}$  (NMTU). This finding further supports the assignment of this band.

### B. Elemental balances of the TU experiment

When referring to elemental balances (Table II), one means the total amount of the particular element (C, S, or N) found in the product molecules relative to that in the precursor (in percent), and they can be compared with that of the one performed with the related molecule, TA.<sup>17</sup> Accordingly, one can see that the listed products account for more converted precursor in the current case than for TA ( $\approx 20\%$  vs  $\approx 10\%$ ), suggesting that H-atom reactions are more efficient when TU is concerned. The total amounts of thiols are 3.9, 4.8, 7.6, and 7.9 ppm at the end of the different stages of H atom

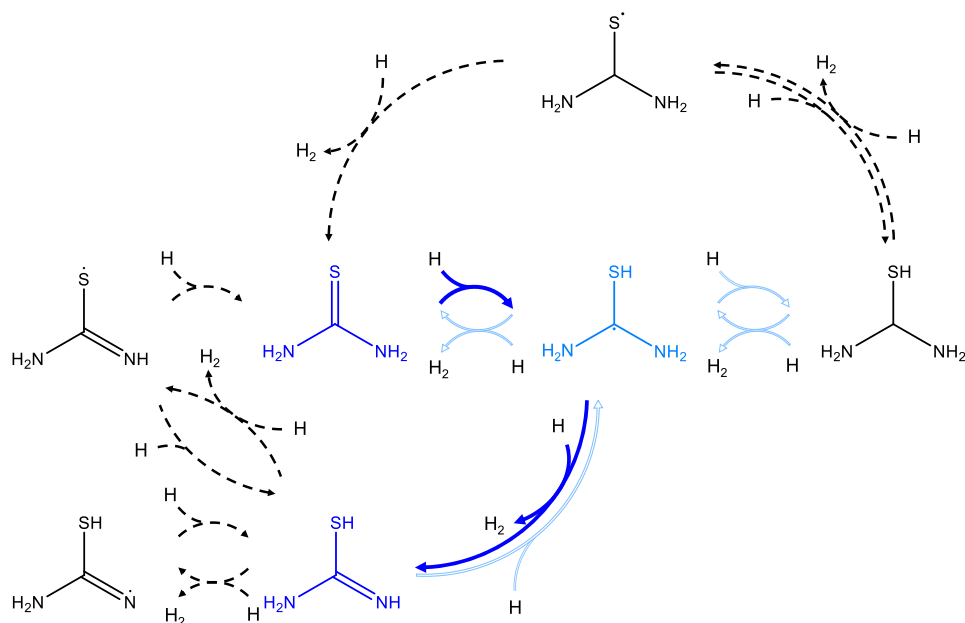


**FIG. 7.** Proposed reaction scheme of the H-atom addition and abstraction reactions of TU upon H atom generation, containing the principal (barrierless) pathways only. For the sake of clarity, reaction channels involving the elimination of H<sub>2</sub>S are not included. Molecules in dark blue were undoubtedly detected, whereas the ones in light blue were assigned tentatively. The bold dark blue arrows indicate the most likely reaction channels, the empty light blue arrows mark potentially important processes without any experimental proof for their occurrence, whereas dotted black arrows specify other, expectedly unimportant channels.

**TABLE II.** Change in mixing ratios (in ppm) of the precursor and the products starting from TU at different stages of H atom generation.

Species	$\Delta$ mixing ratio			
	First 2217 nm	Dark period	Second 365 nm	Second 2217 nm
Precursor	-22.4	-37.1	-35.3	-44.4
<i>s,t</i> -thiol	3.2	3.8	6.1	6.5
<i>s,c</i> -thiol	0.7	1.0	1.5	1.4
NH <sub>3</sub>	0.6	1.3	2.6	3.5
C balance <sup>a</sup>	17%	13%	22%	18%
S balance <sup>a</sup>	17%	13%	22%	18%
N balance <sup>a</sup>	20%	15%	29%	22%

<sup>a</sup>When calculating elemental balances, the fact that all forms of TU contain two N atoms and those of NMTU contain two C and two N atoms must be taken into account.

generation (first 2217 nm irradiation, after waiting in the dark, second 365 nm irradiation, and second 2217 nm irradiation). The same values for TA were 4.0 and 5.3 ppm after the first 2217 nm irradiation and after waiting in the dark, respectively, which are comparable to those obtained for TU. However, in the case of TA, more thione was converted (37 and 66 ppm after the first 2217 nm irradiation and after waiting in the dark, respectively),<sup>17</sup> which may explain the lower elemental balance values. Interestingly, the mixing ratio of NH<sub>3</sub> is also comparable in the two cases. The relative concentration of H-atom-reaction products becomes lower during the dark period, which is in accordance with what was found for TA.<sup>17</sup> This phenomenon may be caused by the more efficient occurrence of alternative reactions, such as the formation of complexes with HCl. The change in the relative rates of competing reactions (like the one involving the elimination of H<sub>2</sub>S, which cannot be detected due to

its extremely weak IR absorption) may also be held accountable for this observation.

The mixing ratio of the tentatively assigned H<sub>2</sub>N- $\dot{C}$ (-SH)-NH<sub>2</sub> can be estimated if one assumes an average IR intensity of  $\approx 150 \text{ km mol}^{-1}$ . Nevertheless, the concentration of this species can only be determined at the end of the first 2217 nm irradiation and after waiting in the dark, as the interference with the absorption of atmospheric CO<sub>2</sub> becomes too strong after that. The corresponding values are 6.0 and 6.7 ppm, significantly less than in the case of TA (10 and 30 ppm).<sup>17</sup> Nonetheless, they still raise the elemental balances to 44% (C and S balance) as well as 46% (N balance) after the first 2217 nm irradiation and 31% (C and S balance) as well as 33% (N balance) after keeping the sample in the dark. This somewhat contradicts what was observed in the TA experiment, where the mixing ratio of the related radical increased monotonously throughout the dark period, in contrast to the constant nature of the mixing ratio observed in the current experiment.

Due to the *para*-H<sub>2</sub> + Cl  $\rightarrow$  HCl + H reaction occurring during the 2217 nm irradiation, the mixing ratio of the generated H atoms can be determined indirectly by using the integrated area of the 2895 cm<sup>-1</sup> HCl band. The values are 978, 1159, 1186, and 1513 ppm after the first 2217 nm irradiation, waiting in the dark, the second 365 nm irradiation, and the second 2217 nm irradiation. The higher mixing ratio of the H atoms in this experiment may account for the different behavior of the radical in the current experiment, as there are more generated H atoms than in the TA experiment (788 and 985 ppm after the first 2217 nm irradiation and waiting in the dark, respectively),<sup>17</sup> facilitating further H-atom reactions taking place on the radical. It is also worth noting that  $\approx 100$ – $200$  H atoms are necessary to produce one product molecule. This is in agreement with our previous results, which also made an attempt to rationalize the apparent lack of efficiency when it comes to H-atom reactions.<sup>17</sup> Finally, one should note that the elemental balances listed in Table II

are lower (except for the S atom) than when the sample is exposed to UV irradiation.

Although the molar balances cannot be calculated for NMTU, a few conclusions can still be drawn. The overall decrease in the thione monomer after the first 2217 nm irradiation and after waiting in the dark is determined to be 14.5 and 26.1 ppm, roughly two-thirds of that of TU (Table II). The mixing ratio of the radical is found to be 8.7 and 10.3 ppm, respectively, which are somewhat higher than that in the case of TU (6.0 and 6.7 ppm). However, the concentration of the generated H atoms is calculated to be 477 and 573 ppm, which are less than half of the experiment for the TU experiment. As a consequence, fewer H atoms translate into a lower chance for the second (H-atom abstraction) step; therefore, the process stops after the first (H-atom addition) reaction, resulting in a somewhat higher mixing ratio of the intermediate than in the case of TU. In addition, considering the greatly increased number of different thiol conformers compared to that of the TU molecule, these two phenomena may give an explanation for the absence of thiols after H-atom generation in the NMTU-containing matrices.

## VI. CONCLUSION

The conclusions drawn from the experimental observations and the quantum-chemical computations suggest the facile occurrence of thione–thiol tautomerization when H atoms are generated in a *para*-H<sub>2</sub> matrix also containing the sulfurous compounds TU and NMTU in a low concentration. This reaction pathway, unlike the ones involving (broadband) UV irradiation, does not require an external energy source, and it only requires the presence of H atoms. According to the theoretical results, the mechanism can be described as follows: The first step is the barrierless H-atom addition on the S atom of the TU or NMTU thione precursors, yielding the intermediate radicals, which were tentatively identified based on their absorption band near the atmospheric CO<sub>2</sub> peak. Subsequently, the second step involves an H-atom abstraction leading to the formation of the thiol tautomeric forms, whose conformers were successfully detected in the TU-containing samples. There may be several possible explanations for the lack of thiols in the case of NMTU; the two most obvious are the high number of conformers rendering their concentration too low or the less efficient H atom generation due to steric effects. The mechanism laid down above is identical to what was found for the related sulfur-bearing compound, TA, in the same *para*-H<sub>2</sub> environment when exposed to H atoms.<sup>17</sup> Another study showed that TA also undergoes the same thione–thiol tautomerization on the surface when bombarded with H atoms in the bulk (amorphous ice) phase.<sup>18</sup> In other words, the process appears to be independent of the environment. These findings point to the ubiquitous nature of the facile hydrogenation/dehydrogenation of the S atom on this family of molecules rather than a unique feature of one of them. Moreover, the fact that the same tautomerization process takes place simply by the presence of H atoms may also have an astrophysical implication: in the core of dark, cold molecular clouds, the ices persisting on the surface of small dust particles are shielded from the UV originating from nearby stars or galactic cosmic rays. However, H atoms are abundant, and the tautomerization assisted by them is not hindered by the low temperature, as the process has been shown to be barrierless.

## SUPPLEMENTARY MATERIAL

The electronic supplementary material contains sections of the MIR difference spectra of TU as well as NMTU in *para*-H<sub>2</sub> matrix after the first H atom generation; the MIR spectrum of *anti*- and *syn*-NMTU deposited in *para*-H<sub>2</sub>; and text discussing and tables listing the zero-point corrected computed energy levels of the H-atom addition as well as H-abstraction products and the transition states (if any) of TU and NMTU, respectively.

## ACKNOWLEDGMENTS

The authors thank the Hungarian Academy of Sciences (MTA) for funding this research through the Lendület program. The Hungarian Scientific Research Fund (No. OTKA K143196) and the Thematic Excellence Program of the Eötvös Loránd University (No. TKP2021-NKTA-64), both from the fund of the National Research, Development and Innovation Office (NKFIH), are acknowledged. S.G. was supported by the “Bolyai” scholarship of MTA as well as by the “ÚNKP-23-5 New National Excellence Program” of the Ministry for Culture and Innovation (KIM) from the source of NKFIH. B.K. and A.S. were both supported by the “ÚNKP-23-3 New National Excellence Program” of KIM from the source of NKFIH. B.K. was also supported by the “DKÖP-23 Doctoral Excellence Program” of KIM from the source of NKFIH. A.S. was also supported by the “EKÖP-24 University Excellence Scholarship Program” of KIM from the source of NKFIH.

## AUTHOR DECLARATIONS

### Conflict of Interest

The authors have no conflicts to disclose.

### Author Contributions

**Sándor Góbi:** Conceptualization (lead); Data curation (lead); Formal analysis (equal); Funding acquisition (supporting); Investigation (lead); Methodology (lead); Project administration (equal); Supervision (equal); Validation (lead); Visualization (lead); Writing – original draft (lead). **Barbara Keresztes:** Investigation (supporting); Writing – review & editing (supporting). **Anita Schneider:** Investigation (supporting); Writing – review & editing (supporting). **György Tarczay:** Funding acquisition (lead); Project administration (equal); Resources (lead); Supervision (equal); Writing – review & editing (supporting).

## DATA AVAILABILITY

The data that support the findings of this study are available from the corresponding author upon request.

## REFERENCES

- <sup>1</sup>M. J. Nowak, L. Lapinski, H. Rostkowska, A. Leś, and L. Adamowicz, *J. Phys. Chem.* **94**, 7406 (1990).
- <sup>2</sup>R. Steudel and Y. Steudel, *J. Phys. Chem. A* **114**, 4437 (2010).
- <sup>3</sup>N. A. M. Pereira, C. M. Nunes, I. Reva, and R. Fausto, *J. Phys. Chem. A* **125**, 6394 (2021).

- <sup>4</sup>B. Bernhardt, F. Dressler, A. K. Eckhardt, J. Becker, and P. R. Schreiner, *Chem.—Eur. J.* **27**, 6732 (2021).
- <sup>5</sup>T. Bally, *Reactive Intermediate Chemistry* (Wiley, Hoboken, NJ, 2003), Vol. 97, pp. 795–845.
- <sup>6</sup>M. Tsuge and Y.-P. Lee, in *Molecular and Laser Spectroscopy*, edited by V. Gupta and Y. Ozaki (Elsevier, Amsterdam, The Netherlands, 2020), Chap. 5, pp. 167–215.
- <sup>7</sup>T. Kumada, *Phys. Rev. B* **68**, 052301 (2003).
- <sup>8</sup>P. L. Raston and D. T. Anderson, *Phys. Chem. Chem. Phys.* **8**, 3124 (2006).
- <sup>9</sup>P. L. Raston, S. C. Kettwich, and D. T. Anderson, *J. Mol. Spectrosc.* **310**, 72 (2015).
- <sup>10</sup>P. R. Joshi and Y. P. Lee, *J. Am. Chem. Soc.* **146**, 23306 (2024).
- <sup>11</sup>B. Keresztes, B. Azaad, A. Schneiker, S. Góbi, G. Ragupathy, G. Péter Szalay, and G. Tarczay, *Astron. Astrophys.* **689**, A21 (2024).
- <sup>12</sup>H. Rostkowska, L. Lapinski, A. Khvorostov, and M. J. Nowak, *J. Phys. Chem. A* **107**, 6373 (2003).
- <sup>13</sup>H. Rostkowska, L. Lapinski, and M. J. Nowak, *Phys. Chem. Chem. Phys.* **20**, 13994 (2018).
- <sup>14</sup>J. Würmel and J. M. Simmie, *Int. J. Chem. Kinet.* **55**, 731 (2023).
- <sup>15</sup>H. Rostkowska, L. Lapinski, and M. J. Nowak, *Spectrochim. Acta, Part A* **313**, 124139 (2024).
- <sup>16</sup>L. Lapinski, H. Rostkowska, A. Khvorostov, and M. J. Nowak, *Phys. Chem. Chem. Phys.* **5**, 1524 (2003).
- <sup>17</sup>S. Góbi, B. Keresztes, A. Schneiker, and G. Tarczay, *Phys. Chem. Chem. Phys.* **26**, 21589 (2024).
- <sup>18</sup>S. Góbi, I. Reva, G. Ragupathy, G. Tarczay, and R. Fausto, *J. Phys. Chem. C* **128**, 21691 (2024).
- <sup>19</sup>G. Bzásó, I. P. Csonka, S. Góbi, and G. Tarczay, *Rev. Sci. Instrum.* **92**, 124104 (2021).
- <sup>20</sup>P. L. Raston and D. T. Anderson, *J. Chem. Phys.* **126**, 021106 (2007).
- <sup>21</sup>S. C. Kettwich, P. L. Raston, and D. T. Anderson, *J. Phys. Chem. A* **113**, 7621 (2009).
- <sup>22</sup>P. L. Raston, S. C. Kettwich, and D. T. Anderson, *Low Temp. Phys.* **36**, 392 (2010).
- <sup>23</sup>M. J. Frisch, G. W. Trucks, H. B. Schlegel, G. E. Scuseria, M. A. Robb, J. R. Cheeseman, G. Scalmani, V. Barone, G. A. Petersson, H. Nakatsuji, X. Li, M. Caricato, A. V. Marenich, J. Bloino, B. G. Janesko, R. Gomperts, B. Mennucci, H. P. Hratchian, J. V. Ortiz, A. F. Izmaylov, J. L. Sonnenberg, D. Williams-Young, F. Ding, F. Lipparini, F. Egidi, J. Goings, B. Peng, A. Petrone, T. Henderson, D. Ranasinghe, V. G. Zakrzewski, J. Gao, N. Rega, G. Zheng, W. Liang, M. Hada, M. Ehara, K. Toyota, R. Fukuda, J. Hasegawa, M. Ishida, T. Nakajima, Y. Honda, O. Kitao, H. Nakai, T. Vreven, K. Throssell, J. A. Montgomery, Jr., J. E. Peralta, F. Ogliaro, M. J. Bearpark, J. J. Heyd, E. N. Brothers, K. N. Kudin, V. N. Staroverov, T. A. Keith, R. Kobayashi, J. Normand, K. Raghavachari, A. P. Rendell, J. C. Burant, S. S. Iyengar, J. Tomasi, M. Cossi, J. M. Millam, M. Klene, C. Adamo, R. Cammi, J. W. Ochterski, R. L. Martin, K. Morokuma, O. Farkas, J. B. Foresman, and D. J. Fox, *GAUSSIAN 16, Revision A.03*, Gaussian, Inc., Wallingford CT, 2016.
- <sup>24</sup>V. Barone, *J. Chem. Phys.* **122**, 014108 (2004).
- <sup>25</sup>J. Bloino and V. Barone, *J. Chem. Phys.* **136**, 124108 (2012).
- <sup>26</sup>S. Góbi, B. Keresztes, A. Schneiker, and G. Tarczay, *Phys. Chem. Chem. Phys.* **26**, 9963 (2024).
- <sup>27</sup>M. Mengel, B. P. Winnewisser, and M. Winnewisser, *J. Mol. Spectrosc.* **188**, 245 (1998).
- <sup>28</sup>M. Ruzi and D. T. Anderson, *J. Phys. Chem. A* **117**, 9712 (2013).
- <sup>29</sup>S. Góbi, B. Keresztes, A. Schneiker, G. Ragupathy, and G. Tarczay, *J. Chem. Phys.* **160**, 024310 (2024).
- <sup>30</sup>M. E. Fajardo, *Appl. Spectrosc.* **73**, 1403 (2019).
- <sup>31</sup>T. Kobayashi, K. Seki, T. Tanaka, and T. Takayanagi, *Comput. Theor. Chem.* **963**, 256 (2011).